Theor Chem Acc (2005) 113: 212–224
DOI 10.1007/s00214-005-0629-0

REGULAR ARTICLE

Jun Yang · Michael Dolg

Valence basis sets for lanthanide 4f-in-core pseudopotentials adapted for crystal orbital ab initio calculations

Received: 2 December 2004 / Accepted: 2 December 2004 / Published Online: 25 April 2005

Abstract Crystal orbital adapted Gaussian (4s4p3d), (5s5p4d) and (6s6p5d) valence primitive basis sets have been derived for calculating periodic bulk materials containing trivalent lanthanide ions modeled with relativistic energy-consistent 4f-in-core lanthanide pseudopotentials of the Stuttgart-Koeln variety. The calibration calculations of crystalline A-type Pm_2O_3 using different segmented contraction schemes (4s4p3d)/[2s2p2d], (4s4p3d)/[3s3p2d], (5s5p4d)/[2s2p2d], (5s5p4d)/[3s3p3d], (5s5p4d)/[4s4p3d], (6s6p5d)/[2s2p2d], (6s6p5d)/[3s3p3d] and (6s6p5d)/[4s4p4d] are discussed at both Hartree–Fock (HF) and density functional theory (DFT) levels for the investigation of basis set size effects. Applications to the geometry optimization of A-type Ln_2O_3 (Ln = La-Pm) show a satisfactory agreement with experimental data using the lanthanide valence basis sets (6s6p5d)/[4s4p4d] and the standard set 6-311G* for oxygen. The corresponding augmented sets (8s7p6d)/[6s5p5d] with additional diffuse functions for describing neutral lanthanide atoms were applied to calculate atomic energies of free lanthanide atoms for the evaluation of cohesive energies for A-Ln_2O_3 within both conventional Kohn-Sham DFT and the a posteriori-HF correlation DFT schemes.

Keywords Valence basis set · Pseudopotential · Ab initio calculation · Crystal orbital · Lanthanide sesquioxide · Cohesive energy

1 Introduction

The quantum chemistry of systems containing lanthanide elements has received much attention in the past two decades [1–4]. At present theoretical chemistry investigations on systems containing f elements are still a considerable challenge [4–7]. The extremely complex electronic structure of the f-elements (e.g., for lanthanides usually 4f as well as 5d and 6s may be partially occupied in the ground state or rather low-lying excited states), large relativistic effects and strong electron correlations pose considerable difficulties to theoretical work. Traditional wave function-based ab initio approaches accounting for relativity at the all-electron Dirac–Coulomb–Breit level and including electron correlation effects by means of coupled-cluster (CC) or configuration interaction (CI) methods need *h*- or even *i*-functions in the one-particle basis sets to yield accurate results [8]. Such highly correlated state-of-the-art all-electron studies are currently feasible only for atoms by exploiting their spherical symmetry and to our knowledge, the method is not applicable to all lanthanide elements, i.e., only calculations for closed-shell systems, one or two electrons outside a closed shell or one or two holes inside a closed shell, are feasible. In order to be able to treat all lanthanide atoms and, more importantly, to be able to deal also with molecules or periodic solid materials, compromises have to be made with respect to the treatment of relativity and electron correlation.

Among the most successful approaches of relativistic ab initio quantum chemistry applicable to these systems is the effective core potential (ECP) method [9]. In this approach the explicit quantum chemical treatment is restricted to the valence electrons and relativistic effects are usually only implicitly accounted for by a proper adjustment of free parameters in the valence model Hamiltonian. Effective core potentials fall in two categories, i.e., model potentials, which preserve the original nodal structure of the all-electron valence orbitals, as well as pseudopotentials, which work after a formal transformation with pseudo-valence orbitals with simplified nodal structure. For both types consistent sets of ECP parameters have been published for lanthanide elements, e.g., model potentials [10, 11] as well as energy-consistent [12, 13] and shape-consistent [14, 15] pseudopotentials. Dolg and coworkers developed and thoroughly tested energy-consistent pseudopotentials for lanthanum through lutetium [12, 13, 16, 17], which yielded accurate results in molecular

J. Yang (✉) · M. Dolg
Institute of Theoretical Chemistry,
University of Cologne,
Greinstr. 4, D-50939,
Cologne, Germany
E-mail: jyang0@uni-koeln.de

applications. Recently, corresponding atomic natural orbital (ANO) Gaussian valence basis sets [18] and segmentedly contracted valence basis sets [19] were derived for the small-core potentials of the entire lanthanide series.

Thanks to recent achievements in describing and predicting properties of bulk materials, electronic structure calculations have become increasingly important in both condensed matter physics and chemistry motivated by designing and preparing materials with controlled properties. The availability of sophisticated codes and powerful computers has made it entirely possible to undertake ab initio computer experiments [20]. These first-principle calculations were performed usually based on plane-wave basis sets in conjunction with pseudopotential and density functional theory (DFT) techniques in solid state physics. Nowadays, some attention for solid calculations is directed to the crystal orbital (CO) method since the general implementation of Hartree–Fock (HF) LCAO in the program CRYSTAL for the treatment of periodic systems was published more than two decades ago [21–24]. At present no applications of the code to lanthanide or actinide systems have been reported (cited from the website: http://www.crystal.unito.it/Basis_Sets/ptable.html), except for a single study on GdN [25]. For those lanthanide-containing crystalline solids, the ECP method has to be applied mainly in order to eliminate the open 4f shell and the many problems related to it. However, the valence basis sets generated for energy-consistent pseudopotentials of lanthanides for molecular applications cannot be transferred directly to periodic compounds without modifications. The reason is that, frequently, atomic basis sets with diffuse functions give rise to a large overlap between Bloch functions which linearly construct crystal orbitals, and thus not only lead to the wasting of computational resources but also might cause the quasi-linear dependence problems due to numerical limitations [26]. The derivation of systematic lanthanide pseudopotential basis sets for solid state calculations is therefore timely.

In this contribution, HF energy-optimized Gaussian valence basis sets for trivalent lanthanum through lutetium ions were derived and adapted for crystal orbital calculations using Stuttgart–Koeln energy-consistent pseudopotentials. In order to eliminate a large part of the difficulties in terms of the partially occupied lanthanide 4f shell, we adopt a 4f-in-core pseudopotential approach [12,27]. The quality of these basis sets were verified by performing calculations for A-type crystalline lanthanide sesquioxides Ln_2O_3(Ln = La–Pm) and comparing the calculated geometries and cohesive energies with experimental results. The calibration investigations for A-Ln_2O_3 were achieved within both HF and DFT schemes using the code CRYSTAL2003 [26]. We selected the light lanthanides as test cases since molecular calculations revealed that for them the errors of the pseudopotentials are larger than for the heavier lanthanides [3]. To the best of our knowledge, no previous systematic work has been found for the customization of lanthanide valence basis sets adapted for crystal orbitals.

Our paper is organized as follows: in Sect. 2, we outline the applied ab initio pseudopotentials and the computational procedure for both HF and DFT. In Sect. 3, we present our results and compare them with the available experimental data to display what accuracy the present HF and DFT approaches can actually achieve. Finally, in Sect. 4, we briefly give our conclusions.

2 Method

We use energy-consistent scalar-relativistic ab initio pseudopotentials to reduce the computational effort and to incorporate the most important relativistic effects. The method of relativistic energy-consistent ab initio ECPs is described in detail elsewhere [12,13] and will be outlined here only briefly. The valence-only model Hamiltonian for an atom or ion with n valence electrons is given as

$$H_v = -\frac{1}{2}\sum_i^n \Delta_i + \sum_{i<j}^n \frac{1}{r_{ij}} + V_{\mathrm{av}}.$$

Here i and j are electron indices. V_{av} denotes a spin-orbit averaged relativistic ECP in a semilocal form for a core with charge Q

$$V_{\mathrm{av}} = -\sum_i^n \frac{Q}{r_i} + \sum_i^n \sum_{\mathrm{lk}} A_{\mathrm{lk}} \exp(-a_{\mathrm{lk}} r_i^2) P_l.$$

P_l is the projection operator onto the Hilbert subspace of angular momentum l. The free parameters A_{lk} and a_{lk} are adjusted to reproduce the total valence energies of a multitude of low-lying electronic states of the neutral atom and its ions [13]. Most of the lanthanide ions have a trivalent ground state in the condensed phase, i.e., the electronic configuration $[4d^{10}\ 4f^{n-1}]5s^2\ 5p^6$ (n=1–15 from lanthanum to lutetium; the core is denoted in brackets). Although the 4f-orbitals form an open shell, they are shielded by the more extended and fully occupied 5s and 5p shells from the environment and therefore seem to have a core-like character. Thus mainly the 5d- and 6s-valence orbitals are responsible for the observed chemical behavior of lanthanides [12]. Therefore, the 4f-in-core ECPs for lanthanides were chosen according to the formal oxidation degree of the lanthanide (III) center. Thus, 11 valence electron ECPs were used, i.e., the 1s-4f shells were included in the ECP core, while all others with a main quantum number larger than 4 were treated explicitly (5s5p5d6s ... shells). The reference data used to determine V_{av} have been taken from relativistic all-electron (AE) calculations using the so-called Wood-Boring (WB) scalar-relativistic Hartree–Fock (HF) approach. Both AE WB and ECP calculations have been performed with an atomic finite-difference HF scheme in order to avoid basis set effects in the determination of the ECP parameters.

The routine to generate the Gaussian valence basis sets for lanthanides is described in the following. In order to compare the basis set effects, we have derived three different sets of primitive Gaussian functions (4s4p3d), (5s5p4d)

and (6s6p4d). In order to avoid linear-dependency numerical problems in solid state calculations which are usually caused by too diffuse functions, we simply fixed the most diffuse exponent of each s, p and d set to the value 0.15 in all cases and reoptimized the remaining exponents. According to our experience this choice allows a quite accurate description of the orbital of trivalent lanthanide ions and at the same time does not lead to convergence problems. Lower values should be avoided due to the densely packed nature of many crystalline structures which results in an unpleasant large overlap between basis functions. Firstly, the unpolarized Gaussian primitive (4s4p3d) sets of exponents were energy-optimized using the atomic HF program ATMSCF [28] for the energetically lowest LS states of doubly-charged lanthanide cations with the configuration $[4f^{n-1}]5s^2 5p^6 5d^1$ (the reason that these cations rather than neutral atoms were selected for basis sets customization will be rationalized in the coming Sect. 3). Secondly, s, p and d functions were then added to the (4s4p3d) primitives, yielding (5s5p4d) and (6s6p5d) uncontracted basis sets. The quality of the basis sets was verified by a comparison with numerical finite difference HF calculations for the Ln^{2+} ions carried out with the program MCHF [29] (representing the HF basis set limit).

The crystalline calibration calculations of A-type lanthanide oxides were carried out with the CRYSTAL2003 program package [21–24, 26], using basis sets and methods as indicated in the following. A variety of treatments of exchange and correlation were used: Hartree–Fock theory (HF), where exchange is computed exactly but correlation is neglected, and density functional theory (DFT) within the Kohn–Sham (KS) formalism using the generalized gradient approximation (GGA). Within the DFT scheme, the geometry optimization was performed using the hybrid functional B3LYP [30] and B3PW [30–34]. It has become a routine approach to use pseudopotentials in connection with DFT in recent years, and the results are often quite accurate [35, 36], although most pseudopotentials and the corresponding basis sets have not been designed for such calculations. The different segmented contraction schemes yield the (4s4p3d)/[2s2p2d], (4s4p3d)/[3s3p2d], (5s5p4d)/[2s2p2d], (5s5p4d)/[3s3p3d], (5s5p4d)/ [4s4p3d], (6s6p5d)/[2s2p2d],(6s6p5d)/[3s3p3d] and (6s6p5d)/[4s4p4d] valence basis sets, which were applied in the calculation of A-Pm_2O_3 to investigate the effect of the basis set quality on the final optimized geometry. Uncontracted primitive basis sets (4s4p3d), (5s5p4d) and (6s6p4d) were also tested for the sake of comparison with these contracted basis sets in the case of A-Pm_2O_3. Only the largest basis set (6s6p5d)/[4s4p4d] was chosen to calculate other A-Ln_2O_3 systems based on the work of Pm_2O_3. Due to the present unavailability of f and g functions in the code CRYSTAL2003,[1] no effort was put to generate polarization basis functions with the angular quantum number larger than two. Sets of one and two f functions possibly also suitable for solid state calculations can be found in a previous publication [12]. For the oxygen atoms, the standard 6-311G* Gaussian function basis set was used without any modification for the all-electron calculation (cited from the EMSL Gaussian Basis Set Order Form: http://www.emsl.pnl.gov/forms/basisform.html).

The following tolerances were employed in the evaluation of the infinite Coulomb and Hartree–Fock exchange series: 10^{-6} for the Coulomb overlap, HF exchange overlap, Coulomb penetration and the first exchange pseudo-overlap; 10^{-12} for the second exchange pseudo-overlap at DFT level and 10^{-25} at HF level respectively in order to ensure convergence. This is sufficient to converge structures since tests at tighter tolerances for both DFT (10^{-7}, 10^{-7}, 10^{-7}, 10^{-7}, 10^{-25}) and HF (10^{-7}, 10^{-7}, 10^{-7}, 10^{-7}, 10^{-30}) show that the maximum difference of optimized lattice constant is less than 0.005 Å with much more computational time. The Fock matrix has been diagonalized at 116 k-points within the irreducible Brillouin zone corresponding to a shrinking factor of 10 in the Monkhorst net [37]. The energy differences with respect to calculations performed with a denser net of k-points (288 k-points corresponding to a shrinking factor of 14) are smaller than 0.02 kJ/cell and 0.01 kJ/cell at the DFT and HF level, respectively. In order to improve the convergence, a negative energy shift of 1.0 hartree to the diagonal Fock/KS matrix elements of occupied orbitals was added and maintained after diagonalization thus reducing their coupling to the unoccupied set. A very accurate extra-large grid consisting of 75 radial points and 974 angular points was employed in the DFT calculations, where Becke grid point weights [30] were chosen.

The conjugated gradient (Polak–Ribiere) minimization was applied using a separate ksh-script LoptCG [38] in the full structural optimization with symmetry constraints, and all the calculations were performed with the same set of indexed bielectronic integrals selected from the reference geometry [26] in order to reduce the numerical noise. The total energy tolerance between two subsequent optimization iterations is set to be 10^{-8} hartree so that the convergence is forced to be achieved by norm criteria instead of energy change for reasons of accuracy.

For the evaluation of cohesive energies from atomic energies, the valence basis sets (6s6p5d) were augmented by adding 2s, 1p and 1 d low-exponent Gaussian functions to yield (8s7p6d) primitive sets. The added exponents were optimized using the atomic program ATMSCF [28] for the isolated neutral lanthanide atoms in the $[4f^{n-1}]5s^2 5p^6\ 5d^1 6s^2$ configuration. These additional functions are needed in order to provide an adequate description of the tails of the isolated atom charge density, especially the diffuse doubly occupied 6s shell [39]. The atomic energy of the oxygen atom was obtained by applying the standard 6-311+G* Gaussian functions with one additional low-exponent function for sp shells. Both KS DFT and the so-called a posteriori-HF correlation DFT method implemented in the code CRYSTAL2003 were applied to calculate the cohesive energy of

[1] Although the shell types implemented in CRYSTAL2003 reach the maximum angular quantum number of 3, our test calculation suggests that the program failed to treat f functions at both HF and DFT level due to the basis set linear dependence even for sufficiently large exponents of f functions.

lanthanide sesquioxides. The atomic calculations of Ln and O for the evaluation of the cohesive energy within DFT were performed using the program MOLPRO [40], where only the hybrid functional B3LYP was applied for correlation and exchange corrections with Becke grid point weights [30] since the functional B3PW is not available in the present version of this code. In the a posteriori-HF correlation scheme, HF calculations were performed for the isolated Ln and O atoms as well as A-Ln_2O_3. The subsequent electron correlation correction was obtained as the integral over the unit cell of a function depending on the crystalline Hartree–Fock charge density. The total energy with this a posteriori-HF correlation correction is simply expressed by the summation of the HF energy and the corresponding correlation energy which was evaluated for Wigner–Levy [41], PW-LSD [31–33], P86 [42] and PW-GGA [31–34] correlation-only functionals in conjunction with exact Hartree–Fock exchange.

The experimental cohesive energy of Ln_2O_3 was obtained here from available thermochemical data, i.e., the standard enthalpy of formation for A-Ln_2O_3, gaseous neutral lanthanide atom and gaseous oxygen atom, according to the following reactions:

$$Ln_2O_3(s) \leftrightarrow 2Ln(g) + 3O(g) \quad \Delta E = \Delta E^{exp}_{cohesive}(G.S.), \quad (1)$$

where G.S. is the acronym of *ground state*, i.e., $[4f^{n-1}]5s^2 5p^6 5d^1 6s^2$ for La ($n = 1$) and Ce ($n = 2$) as well as $[4f^n]5s^2 5p^6 6s^2$ for Pr ($n = 3$), Nd ($n = 4$) and Pm ($n = 5$). The above reaction can be equivalently split into three steps:

$$Ln_2O_3(s) \leftrightarrow 2Ln(s) + \tfrac{3}{2}O_2(g)$$
$$\Delta E_1 = -\Delta H^o_f(A - Ln_2O_3; 298\,K), \quad (2)$$

$$\frac{3}{2}O_2(g) \leftrightarrow 3O(g) \quad \Delta E_2 = 3\Delta H^o_f(O; 298\,K), \quad (3)$$

$$2Ln(s) \leftrightarrow 2Ln(g) \quad \Delta E_3 = 2\Delta H^o_f(Ln; 298\,K). \quad (4)$$

Therefore, the experimental cohesive energy is represented as the following expression:

$$\Delta E^{exp}_{cohesive}(G.S.) = 3\Delta H^o_f(O; 298\,K) + 2\Delta H^o_f(Ln; 298\,K) - \Delta H^o_f(A - Ln_2O_3; 298\,K) \quad (5)$$

The originally calculated cohesive energy $\Delta E^{cal}_{cohesive}(5s^2 5p^6 5d^1 6s^2)$ of Ln_2O_3 was derived by subtracting the summation of the corresponding energies of the isolated composing atoms from the energy of the bulk lanthanide oxide. However, since the configuration $[4f^{n-1}]5s^2 5p^6 5d^1 6s^2$ was applied in all cases of our theoretical calculations, an energy correction ΔE^{exp}_{atom} of the state separation between $[4f^{n-1}]5s^2 5p^6 5d^1 6s^2$ and $[4f^n]5s^2\,5p^6\,6s^2$ must be supplemented to $\Delta E^{cal}_{cohesive}(5s^2 5p^6 5d^1 6s^2)$ for systems containing Pr, Nd and Pm according to Eq. (6) in order to obtain the real cohesive energy of bulk Pr_2O_3, Nd_2O_3 and Pm_2O_3calculated with respect to the experimentally observed atomic ground states:

$$\Delta E^{cal}_{cohesive}(G.S.) = \Delta E^{cal}_{cohesive}(5s^2 5p^6 5d^1 6s^2) + 2\Delta E^{exp}_{atom}, \quad (6)$$

where the experimental energy correction ΔE^{exp}_{atom} is -0.0404 a.u./atom for Pr and -0.0617 a.u./atom for Nd respectively [12].

Although the experimental values were measured at 298 K while the calculated ones correspond to 0 K, we omit the thermal conversion for the calculated cohesive energies from 0 K to 298 K. A further approximation of the present calculation is the complete neglect of the zero-point energy contribution to the cohesive energy.

The A-type hexagonal structure of lanthanide sesquioxides has been found from La_2O_3 to Pm_2O_3 [43,44] with the space group P32/m with one formula per unit cell. The metal atoms are in a sevenfold coordination with four oxygens being closer than the other three. The four oxygens are bonded to five and the other three to four metal atoms [45].

3 Results and discussion

3.1 Valence basis sets derived from atomic calculations

In this part, let us first state the reason that we prefer ionic $[4f^{n-1}]5s^2 5p^6 5d^1$ configurations for doubly charged lanthanide cations of La through Lu rather than the neutral atoms to newly generate crystal orbital-adapted valence basis sets. In the 11-electron semicore $5s^2 5p^6 5d^1 6s^2$ of neutral lanthanides, the two electrons of 6s shell and one electron of 5d shell are the main sources of chemical properties in condensed matter. However, a substantial deviation from a purely ionic bonding $Ln_2^{3+}O_3^{2-}$ between lanthanide and the surrounding atoms (e.g. oxygen in Ln_2O_3) was confirmed by a Mulliken population analysis (see Table 1) following bulk SCF calculations of A-Ln_2O_3. One can note from Table 1 that the Ln-5d population is around 1.0 within the DFT scheme and 0.6 within the HF scheme, and the total atomic charge is about 2.0 instead of the formal oxidation state of 3. In other words, only the two electrons from the diffuse Ln-6s shell are transferred to the oxygen neighbors, whereas the one electron in the more compact Ln-5d shell turns to stay in the lanthanide, thus leading to an occupation close to the one used in our optimizations.

The errors in the total valence energies for La through Lu, which were evaluated by comparing algebraic HF calculations on the doubly charged cations to corresponding finite difference results, are shown in Fig. 1. Increasing the size of primitive sets from (4s4p3d) to (6s6p5d) by adding additional s, p and d functions, the maximum error stays below 0.9, 0.09 and 0.05 eV for (4s4p3d), (5s5p4d) and (6s6p5d), respectively. This indicates that only the two larger primitive sets accurately describe the valence orbitals of trivalent lanthanide ions. In addition, the variations of the errors for (6s6p5d) and to a lesser extent also (5s5p4d) along the lanthanide series are much more regular and smooth than for (4s4p3d), so that more reliable comparisons between bulk systems containing different lanthanides are possible. From an analysis of

Table 1 Mulliken shell populations and atomic charges (Q) on Ln (Ln=La–Pm) in A-Ln_2O_3[a]

	s			p			d			Q		
	HF	B3LYP	B3PW	HF	B3LYP	B3PW	HF	B3LYP	B3PW	HF	B3LYP	B3PW
La	2.098	2.136	2.135	6.105	6.129	6.122	0.641	0.984	1.011	2.156	1.751	1.732
Ce	2.098	2.140	2.138	6.102	6.128	6.123	0.644	0.977	1.004	2.157	1.755	1.736
Pr	2.101	2.144	2.142	6.100	6.129	6.123	0.636	0.970	0.996	2.164	1.758	1.739
Nd	2.103	2.146	2.143	6.101	6.130	6.126	0.629	0.962	0.989	2.169	1.762	1.742
Pm	2.104	2.149	2.147	6.101	6.131	6.129	0.619	0.951	0.976	2.176	1.768	1.749

[a]A $5s^25p^65d^16s^2$ (ground state/excited state) valence subconfiguration is considered for the lanthanide elements; 0, 1, 2, 3 and 4 electrons in the 4f shell are attributed to the PP core for La, Ce, Pr, Nd and Pm, respectively. The (6s6p5d)/[4s4p4d] valence basis sets were applied for La through Pm elements. For oxygen atoms, the standard 6-311G* all-electron basis set was applied

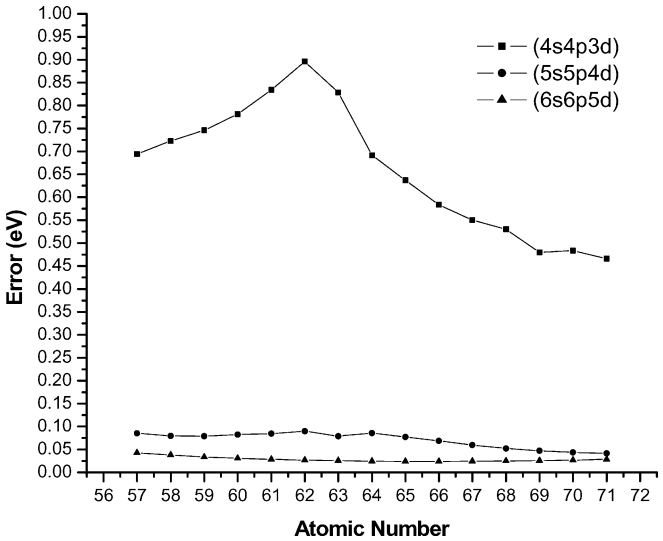

Fig. 1 The total energy difference between the primitive basis set result[a] and the HF limit[b] along the lanthanide series for doubly charged cations with a $[4f^{n-1}]5s^25p^65d^1$ valence configuration [a]Restricted SCF calculations using the program ATMSCF [29]. [b]Numerical finite difference calculations using the program MCHF [30]

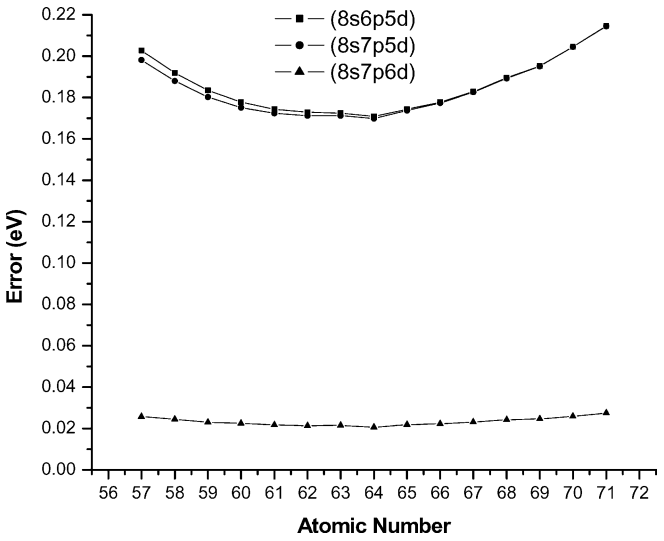

Fig. 2 The total energy difference between the augmented primitive basis set result[a] and the HF limit[b] along the lanthanide series for neutral atoms with the $[4f^{n-1}]5s^25p^65d^1\ 6s^2$ valence configuration [a]cf. footnote a in Fig. 1. [b]cf. footnote b in Fig. 1

the exponents and coefficients of the (4s4p3d) sets we conclude that 3d-functions are not sufficient to describe the 5d pseudo-orbital accurately. The peak in Fig. 1 is related to two different sets of solutions which yield the lowest energy in the beginning and end of the series, respectively. In the case of the sets (6s6p5d), the errors vary only very slightly across the lanthanide series and exhibit a local minimum for Tb. However, the opposite and much stronger variation is observed for the basis sets (4s4p3d) where a pronounced local maximum occurs at Sm. This opposite variation in the total energy for (4s4p3d) is in line with that in the 5d orbital energy (not illustrated here), which indicates that an additional d function is necessary to provide an adequate description of the 5d orbital.

The evaluation of cohesive energies needs valence basis sets with diffuse functions which describe the tails of the charge density on the isolated atoms, e.g., especially the diffuse doubly occupied 6s shell. The errors in the total energy for neutral La through Lu, as illustrated in Fig. 2, were obtained in the same way as for the case of doubly charged cations without diffuse functions. As one can see from Fig. 2, the basis sets (8s7p5d) with two additional s and one additional p functions lead to similar errors compared with the basis sets (8s6p5d). Although the diffuse p function has almost no effect for the atomic HF energy, it is indispensable for the description of the $6s^2 \rightarrow 6p^2$ near-degeneracy. An additional diffuse d function dramatically reduces the errors to less than 0.03 eV nearly by a factor of ten. Furthermore, the variation of errors for (8s7p6d) is much more regular.

When augmenting the contracted (6s6p5d)/[4s4p4d] and (6s6p5d)/[3s3p3d] sets by 2s1p1d diffuse sets, a lower valence energy and a more regular variation of the error in the total valence energies of the $[4f^{n-1}]5s^25p^65d^16s^{22}$ D valence state is obtained than with the original (7s6p5d)/[5s4p3d] valence basis sets [12], cf. Fig. 3. A similar behavior is observed for the (5s5p4d)/[4s4p3d] and (5s5p4d)/[3s3p3d] sets, although the errors are slightly larger. The corresponding (8s7p6d)/[6s5p5d], (8s7p6d)/[5s4p4d] and (7s6p5d)/[6s5p4d], (7s6p5d)/[5s4p4d] sets are most likely also suitable for molecular calculations and supplement the original (7s6p5d)/[5s4p3d] sets. We do not offer diffuse sets for the basis sets based on the (4s4p3d) primitive sets, due to the too large errors observed in the doubly charged cations valence energies

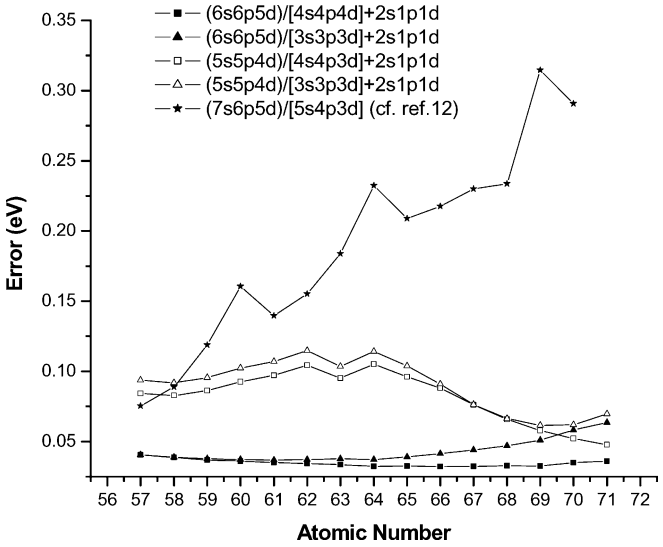

Fig. 3 The total energy difference between the results of contracted basis sets with the augmentation sets 2s1p1d [a] and the HF limit[b] along the lanthanide series for neutral atoms with the $[4f^{n-1}]5s^25p^65d^16s^2$ valence configuration [a]cf. footnote a in Fig. 1. [b]cf. footnote b in Fig. 1

(cf. above), which also affect the total energies of the neutral atoms at a similar magnitude despite the added diffuse functions. Moreover, due to the poor performance for crystal geometry data (cf. below) we do not offer diffuse sets for the [2s2p2d] contractions in case of all primitive sets.

3.2 Calibration calculations of crystalline A-Ln_2O_3

3.2.1 Geometry

3.2.1.1 HF scheme The crystalline calibration calculations for A-type lanthanide sesquioxides Ln_2O_3 were performed using the newly generated valence basis sets at both HF and DFT level in order to verify the transferability of the basis sets from atoms to bulk materials. First, we applied these basis sets at the HF level combined with different contractions to the arbitrarily selected Pm_2O_3, since the other lanthanide sesquioxides are isostructural. The optimized geometry within the HF framework is listed in Table 2. The deviations of lattice constants and bond lengths from the experimental results are, for the largest uncontracted set (6s6p5d), 0.067 Å for a, 0.200 Å for c, 0.074 Å for Pm1–O1 and −0.014 Å for Pm2–O1. Quite similar results were obtained for the smaller uncontracted sets (5s5p4d) and (4s4p3d). This implies that the lattice constants and the bond length Pm1–O1 are substantially overestimated but the bond length Pm2–O1 is slightly underestimated. These relatively large discrepancies between calculated and experimental values are not surprising and are partially due to the lack of electron correlation within the HF treatment. For coordinatively saturated molecular close-shell systems including transition metals, the corresponding deviations were found to even exceed ±0.1 Å for bond distances involving the metal centers [46].

All derived contracted sets, except the [2s2p2d] sets, yield results in good agreement with those of the underlying uncontracted sets. We note here in passing that the seemingly good performance of the [2s2p2d] contraction (e.g. for the lattice constant c) is mostly due to an error cancellation, i.e., basis set incompleteness and neglect of core polarization effects, cf. below. For each case of primitive basis set in Table 2, i.e., (4s4p3d), (5s5p4d) or (6s6p5d) individually, the tightest contraction [2s2p2d] leads to the largest deviation with the differences of 0.043, 0.056 and 0.055 Å, respectively, at its maximum among the lattice constants and bond lengths, compared to the results obtained for uncontracted basis sets. But when loosening the contraction from [2s2p2d] to [3s3p2d] (or [3s3p3d] for (5s5p4d) and (6s6p5d)) as well as to [4s4p3d] (or [4s4p4d] for (6s6p5d)), the geometry is converged within much smaller maximum-differences of only 0.005, 0.008 and 0.007 Å. Therefore, it is clear that although the contraction [2s2p2d] requires less CPU time in calculating condensed matters, this advantage is overthrown by the poor performance in predicting the geometries due to its lower flexibility to properly describe the change of electron density from an isolated ion to the ion in bulk materials.

On the other hand, very similar geometrical parameters are observed for the same basis set contraction among different primitive sizes. For example, for the tightest contraction [2s2p2d], the lattice constants a, c and the bond lengths Pm1–O1, Pm2–O1 are respectively 3.851, 6.101, 2.412 and 2.312 Å at its average with the maximum differences of 0.002, 0.008, 0.005, and 0.001 Å for all primitive sets, i.e., (4s4p3d), (5s5p4d) and (6s6p5d). This is originally caused by the nature of the crystal orbital $\psi_i(r;k)$ in periodic systems, which is the linear combination of Bloch functions $\phi_\mu(r;k)$ other than contracted Gaussian functions (Eq. 7). Each Bloch function is defined as the summation of the same type of atomic orbitals (AO, $\varphi_\mu(r-A_\mu-g)$) translated over the infinite lattice with each AO multiplied by a plane-wave term (Eq. 8), which are expressed as linear combinations of a certain number of our generated primitive Gaussian functions (Eq. 9). Therefore, the real basis sets are ultimately Bloch functions due to the reason that the combination coefficients $a_{\mu,i}$ are actually involved in the variational procedure and contribute to the calculations of density matrix elements. Since the contraction scheme is maintained, the variational freedom stays constant, and Bloch functions are not so sensitive to the increasing size of primitive Gaussian functions from (4s4p3d) to (6s6p5d) due to the plane-wave term $e^{ik\cdot g}$, although more primitives provide a better description of atomic orbitals.

$$\psi_i(r;k)=\sum_\mu a_{\mu,i}(k)\phi_\mu(r;k) \tag{7}$$

$$\phi_\mu(r;k)=\sum_g \varphi_\mu(r-A_\mu-g)e^{ik\cdot g} \tag{8}$$

$$\varphi_\mu(r-A_\mu-g)=\sum_j^{n_G} d_j G(\alpha_j;r-A_\mu-g). \tag{9}$$

As pointed out in Sect. 2., the primitives (6s6p5d) result in a more regular and smooth variation of the calculated energy

Table 2 Lattice constants *a* (Å), *c* (Å), bond lengths Pm1–O1 (Å), Pm2–O1 (Å), bond angles Pm1–O1–Pm2 (°) and O1–Pm2–O1 (°) for Pm_2O_3 from HF pseudopotential calculations using valence basis sets (4s4p3d) (*a*), (5p5s4d) (*b*) and (6s6p5d) (*c*) with different contraction schemes[a]

(4s4p3d)	[2s2p2d]	[3s3p2d]		Uncontracted
a	3.852	3.869		3.867
c	6.098	6.148		6.141
Pm1–O1	2.409	2.425		2.424
Pm2–O1	2.313	2.325		2.323
Pm1–O1–Pm2	105.96	106.03		106.05
O1–Pm2–O2	74.04	73.97		73.95
(5s5p4d)	[2s2p2d]	[3s3p2d]	[4s4p3d]	Uncontracted
a	3.850	3.871	3.870	3.868
c	6.106	6.157	6.154	6.162
Pm1–O1	2.414	2.427	2.430	2.433
Pm2–O1	2.312	2.325	2.324	2.323
Pm1–O1–Pm2	105.97	106.02	105.97	106.01
O1–Pm2–O2	74.03	73.98	74.03	73.99
(6s6p5d)	[2s2p2d]	[3s3p3d]	[4s4p4d]	Uncontracted
a	3.851	3.876	3.870	3.869
c	6.099	6.150	6.152	6.154
Pm1–O1	2.413	2.425	2.428	2.426
Pm2–O1	2.312	2.328	2.324	2.324
Pm1–O1–Pm2	105.95	105.93	105.95	105.96
O1–Pm2–O2	74.05	74.07	74.05	74.04

[a]The experimental values are 3.802 Å (*a*), 5.954 Å (*c*), 2.352 Å (Pm1–O1), 2.338 Å (Pm2–O1), 110.11° (Pm1–O1–Pm2) and 69.89° (O1–Pm2–O2) [54]

Table 3 Lattice constants *a* (Å), *c* (Å), bond lengths Ln1–O1 (Å), Ln2–O1 (Å), bond angles Ln1–O1–Ln2 (°) and O1–Ln2–O1 (°) for Ln_2O_3(Ln = La–Pm) from HF pseudopotential calculations using valence basis sets (6s6p5d)/[4s4p4d]

(6s6p5d)/[4s4p4d]	La_2O_3	Ce_2O_3	Pr_2O_3	Nd_2O_3	Pm_2O_3
a					
Cal.	3.993	3.960	3.928	3.897	3.870
PAW[a]	3.936	3.941	3.895	3.859	3.819
Exp[b]	3.934	3.891	3.859	3.827	3.802
c					
Cal.	6.313	6.264	6.226	6.189	6.152
PAW[a]	6.166	6.182	6.126	6.072	6.023
Exp[b]	6.136	6.059	6.013	5.991	5.954
Ln1–O1					
Cal.	2.486	2.472	2.456	2.442	2.428
PAW[a]	2.457	2.452	2.428	2.406	2.387
Exp[b]	2.457	2.434	2.461	2.391	2.352
Ln2–O1					
Cal.	2.399	2.378	2.359	2.340	2.324
PAW[a]	2.368	2.370	2.342	2.320	2.296
Exp[b]	2.365	2.339	2.305	2.300	2.338
Ln1–O1–Ln2					
Cal.	106.10	105.99	105.98	105.98	105.95
PAW[a]	106.29	106.24	106.24	106.18	106.16
Exp[b]	106.20	106.17	104.84	106.08	110.11
O1–Ln2–O2					
Cal.	73.90	74.01	74.02	74.02	74.05
PAW[a]	73.71	73.76	73.76	73.82	73.84
Exp[b]	73.80	73.83	75.16	73.92	74.04

[a]The geometry was optimized by Hirosaki et al. [48] performing ab initio calculations based on DFT with the PW91 functional using the projector augmented-wave pseudopotential method (PAW), where the localized 4f shell was treated as a core-like shell
[b]The experimental data are cited from the reference [57] (La_2O_3), [58] (Ce_2O_3), [59] (Pr_2O_3), [60] (Nd_2O_3) and [54] (Pm_2O_3)

for free doubly charged lanthanide cations along the lanthanide series. Therefore we further applied only the valence basis set (6s6p5d)/[4s4p4d] to the other A-Ln_2O_3 crystalline compounds for geometry optimizations. The obtained geometrical parameters and the available experimental results are listed and compared in Table 3. We note that the bond angles agree very well with both the plane-wave pseudopotential calculations and the experimental results, whereas somewhat larger deviations of lattice constants and bond lengths are found.

Table 4 Lattice constants *a* (Å), *c* (Å), bond lengths Pm1–O1 (Å), Pm2–O1 (Å) and bond angles Pm1–O1–Pm2 (°), O1–Pm2–O1 (°) for Pm_2O_3 from DFT pseudopotential calculations using valence basis sets (4s4p3d) (*a*), (5p5s4d) (*b*) and (6s6p5d) (*c*) with different contraction schemes

(4s4p3d)	[2s2p2d]	[3s3p2d]		Uncontracted	Exp[a]	PAW[b]
a	3.842	3.864		3.864	3.802	3.819
	3.822	3.844		3.842		
c	6.067	6.136		6.128	5.954	6.023
	5.984	6.052		6.050		
Pm1–O1	2.397	2.418		2.417	2.352	2.387
	2.375	2.394		2.395		
Pm2–O1	2.309	2.324		2.323	2.338	2.296
	2.297	2.311		2.310		
Pm1–O1–Pm2	106.15	106.28		106.20	110.11	106.16
	106.08	106.19		106.18		
O1–Pm2–O2	73.85	73.72		73.80	69.89	73.84
	73.92	73.81		73.82		
(5s5p4d)	[2s2p2d]	[3s3p3d]	[4s4p3d]	Uncontracted	Exp.[a]	PAW.[b]
a	3.839	3.869	3.865	3.864	3.802	3.819
	3.820	3.847	3.845	3.844		
c	6.076	6.136	6.138	6.141	5.954	6.023
	5.987	6.050	6.050	6.049		
Pm1–O1	2.399	2.416	2.421	2.423	2.352	2.387
	2.376	2.393	2.397	2.397		
Pm2–O1	2.308	2.326	2.324	2.323	2.338	2.296
	2.296	2.313	2.311	2.310		
Pm1–O1–Pm2	106.20	106.22	106.18	106.19	110.11	106.16
	106.11	106.16	106.11	106.09		
O1–Pm2–O2	73.80	73.78	73.82	73.81	69.89	73.84
	73.89	73.84	73.89	73.91		
(6s6p5d)	[2s2p2d]	[3s3p3d]	[4s4p4d]	Uncontracted	Exp.[a]	PAW.[b]
a	3.841	3.869	3.865	3.866	3.802	3.819
	3.822	3.849	3.846	3.844		
c	6.066	6.146	6.148	6.134	5.954	6.023
	5.986	6.054	6.048	6.057		
Pm1–O1	2.397	2.418	2.422	2.418	2.352	2.387
	2.374	2.393	2.394	2.396		
Pm2–O1	2.309	2.326	2.324	2.324	2.338	2.296
	2.297	2.308	2.311	2.310		
Pm1–O1–Pm2	106.16	106.20	106.21	106.15	110.11	106.16
	106.10	106.16	106.06	106.11		
O1–Pm2–O2	73.84	73.80	73.79	73.85	69.89	73.84
	73.90	73.84	73.94	73.89		

Two calculated geometrical parameters are presented in each box with the first one obtained from B3LYP followed by the second one obtained from B3PW

[a]The experimental data are cited from the Ref. [56]

[b]cf. footnote a in Table 3

3.2.1.2 DFT scheme Let us now turn to discuss the results obtained within the framework of DFT. First we tested the valence basis sets with different contractions only for A-Pm_2O_3, where the currently popular hybrid functionals B3LYP and B3PW were applied as recommended for geometry optimizations by Koch and Holthausen [47]. We compare the calculated geometries in Table 4 in the same way as for HF calculations in Table 2. Compared with the experimental results, the deviations of lattice constants and bond lengths are, for the largest uncontracted sets (6s6p5d), 0.064 Å for *a*, 0.080 Å for *c*, 0.066 Å for Pm1–O1 and −0.014 Å for Pm2–O1 in B3LYP as well as 0.042 Å for *a*, 0.097 Å for *c*, 0.044 Å for Pm1–O1 and −0.028 Å for Pm2–O1 in B3PW. Both functionals perform better than the HF method.

Similar to the HF case, the tightest contraction [2s2p2d] yield results closest to the experimental values, e.g., for (6s6p5d)/[2s2p2d] the derivations are 0.039 Å (*a*), 0.112 Å (*c*), 0.045 Å (Pm1–O1), and −0.029 (Pm2–O1) for B3LYP as well as 0.020 Å (*a*), 0.032 Å (*c*), 0.022 Å (Pm1–O1), and −0.041 Å (Pm2–O1) for B3PW. However, for each case of the primitive basis set in Table 4, i.e., (4s4p3d), (5s5p4d) or (6s6p5d) individually, the tightest contraction [2s2p2d] leads to the largest deviations with the differences of 0.061 Å, 0.065 Å and 0.078 Å for B3LYP as well as 0.066 Å, 0.061 Å and 0.071 Å for B3PW at its maximum among the lattice constants and bond lengths, compared with the results from the uncontracted sets. But when loosening the contraction from [2s2p2d] to [3s3p2d] ([3s3p3d] for (5s5p4d) and (6s6p5d)) as well as to [4s4p3d] ([4s4p4d] for (6s6p5d)), the geometry is converged within much smaller maximum differences of only 0.008 Å, 0.007 Å and 0.012 Å for B3LYP and 0.002 Å, 0.004 Å and 0.009 Å for B3PW. In addition, for example,

Table 5 Lattice constants *a* (Å), *c* (Å), bond lengths Ln1–O1 (Å), Ln2–O1 (Å), bond angles Ln1–O1–Ln2 (°) and O1–Ln2–O1 (°) for Ln_2O_3 (Ln = La–Pm) from DFT pseudopotential calculations using valence basis sets (6s6p5d)/[4s4p4d] and the hybrid functional B3PW

B3PW (6s6p5d)/[4s4p4d]	La_2O_3	Ce_2O_3	Pr_2O_3	Nd_2O_3	Pm_2O_3
a					
Cal.	3.967	3.935	3.902	3.873	3.846
PAW[a]	3.936	3.941	3.895	3.859	3.819
Exp[b]	3.934	3.891	3.859	3.827	3.802
c					
Cal.	6.208	6.156	6.121	6.082	6.048
PAW[a]	6.166	6.182	6.126	6.072	6.023
Exp[b]	6.136	6.059	6.013	5.991	5.954
Ln1–O1					
Cal.	2.457	2.437	2.422	2.408	2.394
PAW[a]	2.457	2.452	2.428	2.406	2.387
Exp[b]	2.457	2.434	2.461	2.391	2.352
Ln2–O1					
Cal.	2.385	2.365	2.345	2.327	2.311
PAW[a]	2.368	2.370	2.342	2.320	2.296
Exp[b]	2.365	2.339	2.305	2.300	2.338
Ln1–O1–Ln2					
Cal.	106.16	106.10	106.11	106.10	106.06
PAW[a]	106.29	106.24	106.24	106.18	106.16
Exp[b]	106.20	106.17	104.84	106.08	110.11
O1–Ln2–O2					
Cal.	73.84	73.90	73.89	73.60	73.94
PAW[a]	73.71	73.76	73.76	73.82	73.84
Exp[b]	73.80	73.83	75.16	73.92	74.04

[a] cf. footnote a in Table 3
[b] cf. footnote b in Table 3

for the tightest contraction [2s2p2d] of all primitive sets, i.e. (4s4p3d), (5s5p4d) and (6s6p5d), the lattice constant *a*, *c* and the bond length Pm1–O1, Pm2–O1 are respectively 3.841 Å, 6.070 Å and 2.398 Å, 2.309 Å at its average with the maximum differences of 0.003 Å, 0.01 Å and 0.002 Å, 0.001 Å for B3LYP as well as 3.821 Å, 5.986 Å and 2.375 Å, 2.297 Å at its average with the maximum differences of 0.002 Å, 0.003 Å and 0.002 Å, 0.001 Å for B3PW. Therefore, similar valence basis set effects on geometries, as we already pointed out for HF calculations, were observed at DFT level for both B3LYP and B3PW functionals: the calculated geometrical parameters are converged for the [3s3p2d] and other less contracted basis sets and the increasing size of primitive sets from (4s4p3d) to (6s6p5d) results in no apparent variation of final optimized structures. The use of the [2s2p2d] contractions is not recommended. Besides this, as one can see clearly in Table 4, the B3PW results agree much better than those of the B3LYP and HF method with the experimental values and the plane-wave pseudopotential results. In the subsequent calculations, only the valence basis set (6s6p5d)/[4s4p4d] and the hybrid functional B3PW were applied to the other A-Ln_2O_3 crystalline compounds.

The calculated geometries for A-Ln_2O_3 (Ln = La–Pm) at the DFT level are listed in Table 5. The average deviations of geometrical parameters for the five compounds compared with the experimental results are 0.041 Å (*a*), 0.092 Å (*c*), 0.020 Å (Ln1–O1), 0.028 Å (Ln2–O1) and 1.11° (Ln1–O1–Ln2), which are smaller than the corresponding deviations at the HF level, i.e., 0.067 Å (*a*), 0.198 Å (*c*), 0.040 Å (Ln1–O1), 0.036 Å (Ln2–O1) and 1.14° (Ln1-O1-Ln2). The lattice constants and bond lengths obtained from experiment, the projector augmented-wave pseudopotential method (PAW) [48], HF and DFT calculations are respectively plotted in Fig. 4. The DFT results based on the B3PW functional and (6s6p5d)/[4s4p3d] basis sets are closer to the results of the PAW calculations than to the experimental results within the average deviations of 0.017 Å (*a*), 0.022 Å (*c*), 0.006 Å (Ln1–O1), 0.009 Å (Ln2–O1) and 0.10° (Ln1–O1–Ln2) for the five compounds. Furthermore, as illustrated in Fig. 4, our calculated results show a linear correlation for both lattice constants and bond lengths along the atomic number at both HF and DFT levels in agreement with experimental findings and at variance with the irregular variations from La_2O_3 over $Ce_2O_3$to Pr_2O_3 in the PAW calculations. This consistently smooth correlation found in our results favors the reliable comparison of properties between crystalline compounds containing different lanthanide metals. Finally, it is easy to conclude that, based on the above analysis of deviations, our valence basis sets in conjunction with DFT/B3PW provide more accurate characterizations for bond lengths and angles than for lattice constants.

At this point it is fair to mention that the present CRYSTAL calculations do not take into account the full valence model Hamiltonian for the lanthanides, i.e., the core polarization potential (CPP) is missing due to technical reasons. Previous work on molecules revealed that including a CPP to the 4f-in-core ECPs leads to bond length contraction of several hundredths of an Å, thus explaining at least partially the tendency of the current results to overestimate the experimental values [49]. Another reason for the too long bond lengths

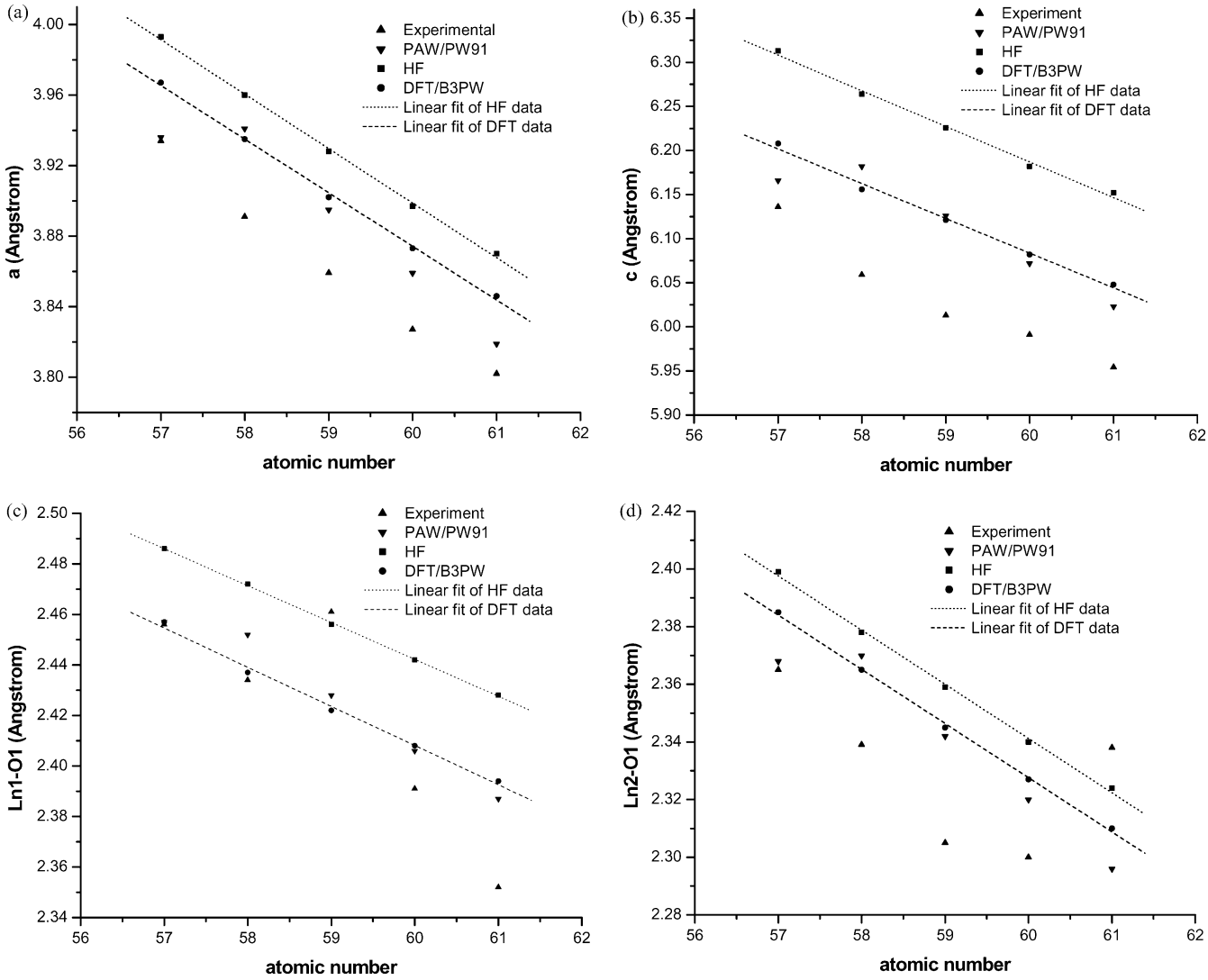

Fig. 4 a–d The variation of geometrical parameters obtained respectively from experiment [54–58], the projector augmented-wave pseudopotential (PAW) method [49], HF and DFT calculations with respect to atomic numbers of lanthanides from La to Pm. The calculated lattice constants a and c as well as bond lengths Ln1–O1 and Ln2–O1 are linearly fitted by *dashed* (DFT) and *dot* (HF) lines in a, b, c and d, respectively

and lattice constants is certainly the omission of f-functions in the basis sets, as it also has been demonstrated previously for molecules [16]. We expect that once the inclusion of f-functions becomes possible, this would improve especially the results for the systems at the beginning of the lanthanide series.

3.2.2 Charge distribution

The Mulliken populations are shown in Table 1. Since the shells with a main quantum number smaller than 5 are taken as effective core potential of Ln, the valence shell electron population has a $5s^2 5p^6 5d^1 6s^2$ configuration as reference (11 electrons). It is well known that the compact 4f-shell shields the nuclear-charge quite efficiently and only small differences are observed in the populations of the outer valence orbitals when comparing neighboring lanthanides. The s-population is about 2.1 no matter what theoretical scheme was applied, which suggests that the 6s orbital acts as the main electron donor in these crystalline compounds. There are only slight differences of the p-population between HF and DFT as well, which is about 6.1, while the difference of the d-population is substantial: whereas the valence d-electron is almost completely retained on the lanthanide at the DFT level (d-population around 1.0), it is partially transferred to oxygen in the HF case (d-population around 0.6). As a result, HF calculations favor all lanthanide sesquioxides with more ionic and polar metal centers than the DFT scheme. In all schemes the total charge Q increases slightly along the series, which implies that the ionic character of the lanthanide is increased and covalent bonding becomes less important from La to Pm. We note that the charge increase mainly stems from the decrease of the 5d population, which is at least partly due to

Table 6 Cohesive energy of lanthanide sesquioxides at both HF in combination with the a posteriori-HF correlation correction and DFT levels. The comparison with experiment is given in % in bracket. The experimental results for the state $[4f^{n-1}]5s^2\ 5p^6\ 5d^1\ 6s^2$ (n =1–5 for La through Pm respectively) were obtained in the way outlined at the end of Sect. 2. The unavailable experimental data for Pm_2O_3 has been substituted by an estimate (cf. text)

(6s6p5d)/[4s4p4d]	La_2O_3	Ce_2O_3	Pr_2O_3	Nd_2O_3	Pm_2O_3
HF (a.u./cell)	0.9048	0.9114	0.9154	0.9195	0.9250
	(69.8%)	(70.6%)	(73.2%)	(75.8%)	(75.02%)
a posteriori-HF (a.u./cell)					
PW-LSD	1.0616	1.0515	1.0138	0.9951	1.0001
	(81.9%)	(81.4%)	(80.9%)	(81.4%)	(81.1%)
PW-GGA	1.1462	1.1375	1.1007	1.0820	1.0882
	(88.4%)	(88.1%)	(87.9%)	(88.5%)	(88.3%)
P86	1.1508	1.1592	1.1142	1.0955	1.1017
	(89.1%)	(89.4%)	(88.9%)	(89.6%)	(89.4%)
Wigner-Levy	1.2423	1.2336	1.2061	1.1791	1.1815
	(95.8%)	(95.5%)	(96.3%)	(96.5%)	(95.8%)
DFT/B3LYP (a.u./cell)	1.1779	1.1829	1.1455	1.1265	1.1318
	(90.9%)	(91.6%)	(91.4%)	(92.2%)	(91.8%)
Experiment [54, 59, 60] (a.u./cell)	1.2960	1.2914	1.2527	1.2224	1.2330
	(100%)	(100%)	(100%)	(100%)	(100%)

their increasing indirect relativistic destabilization along the lanthanide series. As mentioned in the previous part, the evident covalent contribution to the bonding between lanthanide centers and surrounding oxygens is the main reason that the valence basis sets were generated for the doubly charged lanthanide cations with an occupied 5d orbital rather than for the triply charged cations.

3.2.3 Cohesive energy

The results for the cohesive energies are listed in Table 6. Hartree–Fock calculations for free lanthanide atoms show that in accordance with Hund's rule the ground state within a $4f^{n-1}$ -subconfiguration of La through Pm corresponds to the fully polarized atomic configuration with maximum total spin density, i.e., to $5s^2 5p^6\ 5d^1 6s^2$ for Ln (Ln = La, Ce, Pr, Nd and Pm). When the DFT calculations for free lanthanide atoms are invoked, a slight unphysical orbital mixing happens between s- and d-orbitals, which leads to the fractional occupations, i.e., of $5s^{3.962}5p^6 5d^{1.038}$ for La, $5s^{3.967}5p^6 5d^{1.033}$ for Ce, $5s^{3.972}5p^6 5d^{1.028}$ for Pr, $5s^{3.976}\ 5p^6\ 5d^{1.024}$ for Nd and $5s^{3.980}\ 5p^6\ 5d^{1.020}$ for Pm. This unclean configuration is not technically unexpected partly because the current version of MOLPRO2002 simply does not support non-Abelian point-groups and O_h is thus out of reach to prevent such a mixing and partly because density functional approaches favor states with more d-electrons since more correlation contributions are found in d- than s-orbitals due to the more compact nature [47]. Although it is difficult to estimate the energy loss for lanthanide atoms resulting from the s- and d-orbital mixing, the atomic energy deviation between the fractional and integral occupations is believed to be small since the maximum deviation from integral occupation numbers is only 0.038 electrons.

We note that at the scalar-relativistic all-electron Wood-Boring HF level, all lanthanides La-Pm possess a $[4f^{n-1}]5s^2\ 5p^6 5d^1\ 6s^2$ ground state configuration [12]. Experimentally this is only true for La and Ce, whereas Pr, Nd and Pm have a $[4f^{n}]5s^2 5p^6 6s^2$ ground state configuration [50]. For the latter elements, we thus apply the empirical corrections to the observed ground state as outlined in Ref. [8] for all results which include correlation effects.

It turns out that the cohesive energy estimated at the HF level represents about 70% of the experimental one derived from thermochemical data. To restore the cohesive energy theoretically to an acceptable level, correlation contributions are taken into account in two different ways, i.e., the a posteriori-HF scheme and the conventional KS DFT. The a posteriori-HF correction is very effective in reducing the error in the binding energy to a few per cent according to previous reports on solid calculations [51–53]. Nevertheless, no previous work was found reporting the calculation of cohesive energies for periodic systems containing lanthanide elements using such a correlation correction. However, similar a posteriori-HF correlation corrections were successfully applied to lanthanide atoms using the 4f-in-core pseudopotentials [12]. As one can see in Table 6, the calculated cohesive energies account for ≈81–82% (PW-LSD), ≈88–89% (PW-GGA), ≈89–90% (P86) and ≈95–97% (Wigner–Levy) of the experimental values for the four compounds. Once again, the fact is confirmed in this work that the performance of the local spin-density approximation for correlation PW-LSD is considerably improved by the gradient-corrected functional PW-GGA and P86 in calculating the cohesive energy. In the conventional DFT scheme using B3LYP, ≈90–92% of the experimental values were restored.

Based on these pleasing results, our approach with respect to 4f-in-core pseudopotentials connected with crystal orbital-adapted valence basis sets for lanthanide elements is successful in evaluating cohesive energies of bulk materials and promising for further applications in this area. As one example, we predicted, by means of the method described below, the theoretical value of cohesive energy for the bulk A-type Pm_2O_3 (see the last column in Table 6). This calculation is meaningful since the experimental cohesive energy of Pm_2O_3 has not been available up to now due to

Table 7 The calculated cohesive energy of the bulk A-type Pm_2O_3 at both HF in combination with the a posteriori-HF correlation correction and DFT levels. The valence basis sets (6s6p5d)/[4s4p4d] was applied for Pm atoms, and the standard set 6-311+G* for oxygen atoms. The physical meanings of the parameters in this table can be referred in Sect. 2

a.u./cell	HF (a.u./cell)	a posteriori-HF (a.u./cell)				DFT/B3LYP (a.u./cell)
		PW-LSD	PW-GGA	P86	Wigner-Levy	
$\overline{D}$	70.10%	81.42%	88.23%	89.28%	96.03%	91.52%
$\Delta E^{\text{cal}}_{\text{cohesive}}$ $(5s^25p^65d^16s^2)$	0.9250	1.0609	1.1482	1.1617	1.2415	1.1918
$\Delta E^{\text{cal}}_{\text{cohesive}}$(G.S.)	0.8650 (70.2%)	1.0001 (81.1%)	1.0882 (88.3%)	1.1017 (89.4%)	1.1815 (95.8%)	1.1318 (91.8%)
$\Delta E^{\text{exp}}_{\text{corr}}$			−0.0300			
$\Delta E^{\text{exp}}_{\text{cohesive}}$(G.S.)			1.2330			

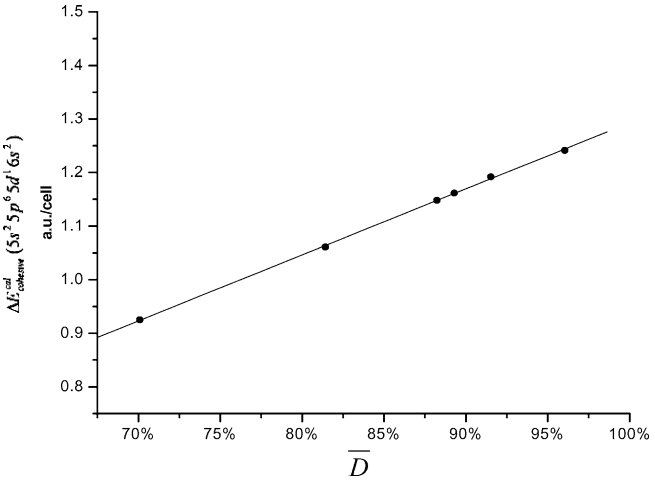

Fig. 5 The linear correlation between the calculated cohesive energy for the configuration $[4f^{n-1}]5s^25p^65d^16s^2$ of atomic Pm and the average deviation $\bar{D}$ among La_2O_3 through Nd_2O_3 in each scheme. The data is linearly fitted by the equation $\Delta E^{\text{cal}}_{\text{cohesive}}(5s^25p^65d^16s^2) = 1.23295\bar{D} + 0.05999$, where the slope 1.23295 a.u./cell stands for the predicted experimental cohesive energy and half of the intercept 0.0300 a.u./atom stands for the energy correction between the state $[4f^{n-1}]5s^25p^65d^16s^2$ and $[4f^n]5s^2\ 5p^6\ 6s^2$ of atomic Pm

the radioactive nature of Pm which decays too fast to be thermochemically measured for Pm_2O_3. It is easy to write the following equations by taking $\Delta E^{\text{cal}}_{\text{cohesive}}(5s^25p^65d^16s^2)$, $\Delta E^{\text{cal}}_{\text{cohesive}}$ (G.S.), $\Delta E^{\text{exp}}_{\text{cohesive}}$ (G.S.), $\Delta E^{\text{exp}}_{\text{corr}}$ and the average deviation $\bar{D}$ as parameters. The physical meanings of these parameters in Eqs. (10) and (11) have been introduced in Sect. 2.

$$\Delta E^{\text{cal}}_{\text{cohesive}}(\text{G.S.}) = \Delta E^{\text{cal}}_{\text{cohesive}}(5s^25p^65d^16s^2) + 2\Delta E^{\text{exp}}_{\text{corr}}. \quad (10)$$

$$\Delta E^{\text{cal}}_{\text{cohesive}}(\text{G.S.}) = \Delta E^{\text{exp}}_{\text{cohesive}}(\text{G.S.}) \cdot \overline{D}. \quad (11)$$

According to Eqs. (10) and (11), the correlation is derived in Eq. (12):

$$\Delta E^{\text{cal}}_{\text{cohesive}}(5s^25p^65d^16s^2) = \Delta E^{\text{exp}}_{\text{cohesive}}(\text{G.S.}) \cdot \overline{D} - 2\Delta E^{\text{exp}}_{\text{corr}}. \quad (12)$$

As a result, since $\Delta E^{\text{exp}}_{\text{cohesive}}$ (G.S.) and $\Delta E^{\text{exp}}_{\text{corr}}$ are constants for Pm_2O_3 and Pm, respectively, the linear correlation between $\Delta E^{\text{cal}}_{\text{cohesive}}(5s^25p^65d^16s^2)$ and $\bar{D}$ yields thus as the slope and half of the intercept of this straight line the experimental cohesive energy for the bulk Pm_2O_3 and the atomic energy correction of state separation for neutral atomic Pm, respectively. The theoretical cohesive energy $\Delta E^{\text{cal}}_{\text{cohesive}}$ $(5s^2\ 5p^6\ 5d^16s^2)$ of Pm_2O_3 for the configuration $[4f^{n-1}]5s^25p^6\ 5d^16s^2$ is calculated in the same way as for La_2O_3 through Nd_2O_3. The deviation $\bar{D}$ is evaluated by averaging the values in parentheses of each row in Table 6 from La_2O_3 to Nd_2O_3. The plot of $\Delta E^{\text{cal}}_{\text{cohesive}}(5s^25p^65d^16s^2)$ against $\bar{D}$ is illustrated in Fig. 5. Therefore, the calculated cohesive energy of bulk Pm_2O_3 with respect to the ground states is found to be 1.2330 a.u./cell with the byproduct of an energy separation of −0.82 eV/atom for atomic Pm between the configurations $[4f^n]5s^25p^66s^2$ and $[4f^{n-1}]5s^25p^6\ 5d^16s^2$. In view of the −0.84 eV/atom energy separation found experimentally for the neighbor element Nd and the closeness of the corresponding HF and WB all-electron values of Nd and Pm [12], the latter result seems to be reasonable.

4 Conclusions

Optimized crystal orbital adapted valence basis sets for lanthanide 4f-in-core energy-consistent pseudopotentials describing the configuration $[4d^{10}\ 4f^{n-1}]5s^25p^65d^16s^2$ of trivalent lanthanides in periodic systems were presented and tested in bulk calibration calculations for some selected model crystalline A-type lanthanide sesquioxides. The mean absolute errors in the HF energy of Ln^{2+}-$5s^25p^65d^1$ for (4s4p3d), (5s5p4d) and (6s6p5d) primitives are 0.66, 0.070 and 0.028 eV, respectively. The mean absolute errors are slightly decreased to 0.023 eV by extending (6s6p5d) to (8s7p6d) with additional diffuse functions necessary to describe the neutral atoms. Our calculations using the newly generated basis sets (6s6p5d)/[4s4p4d] for geometrical parameters of crystalline Ln_2O_3 (Ln = La, Ce, Pr, Nd and Pm) overshoot the experimental ones by less than 1.5% for lattice constants and 1.2% for bond lengths at the DFT/B3PW level, and achieve the average deviation of about 0.4% for lattice constants and 0.2% for bond lengths when compared with the previously reported PAW calculation. The valence basis sets customized for crystalline calculations restore the calculated cohesive energy of Ln_2O_3 (Ln = La-Nd) to more than 88% of

the experimental data within the a posteriori-HF correlation scheme in combination with gradient-corrected functionals. Good agreement has also been found between the conventional DFT results and the experimental cohesive energy with the deviation of only few per cent. The cohesive energy of bulk A-type Pm_2O_3 is also calculated to be 773.72 kcal/mol to fill the gap in experimental data. In future work we will generate corresponding crystal orbital adapted basis sets for the most frequently occurring divalent (e.g. Eu, Yb) and tetravalent (e.g. Ce, Tb) lanthanide elements.

Acknowledgements This work is financially sponsored by the project Graduiertenkolleg 549, "Azentrische Kristalle" at the University of Köln. The authors also acknowledge the support of Deutsche Forschungsgemeinschaft (National Science Foundation of Germany).

References

1. Pyykkö P (1987) Inorg Chim Acta 139:243–245
2. Balasubramanian K (1994) Handbook on the physics and chemistry of rare earths. In: Gschneidner KA Jr, Eyring L (eds). Elsevier, Amsterdam, vol 18, p 29
3. Dolg M, Stoll H (1996) Handbook on the physics and chemistry of rare earths. In: Gschneidner KA Jr, Eyring L (eds). Elsevier, Amsterdam, vol 22, p 607
4. Dolg M (1998) Encyclopedia of computational chemistry. In: Schleyer PVR, Allinger NL, Clark T, Gasteiger J, Kollman PA, Schäfer III HF, Schreiner PR (eds.). Wiley, Chichester, p 1478
5. Pepper M, Bursten B (1991) Chem Rev 91:719–741
6. Schreckenbach G, Hay PJ, Martin RL (1999) J Comput Chem 20:70–79
7. Dolg M, Cao XY (2004) Recent advances in computational chemistry. In: Hirao K, Ishikawa Y (eds). World Scientific Publishing, New Jersey, vol 5, p 1
8. Eliav E, Kaldor U (1995) Phys Rev A 52:291–296
9. Kutzelnigg W (1987) Phys Scr 36:416–431
10. Sakai Y, Miyoshi E, Tatewaki H (1998) J Mol Struct (Theochem) 451:143–150
11. Seijo L, Barandiaran Z, Harguindey E (2000) J Chem Phys 114:118–129
12. Dolg M, Stoll H, Savin A, Preuss H (1989) Theor Chim Acta 75:173–194
13. Dolg M, Stoll H, Preuss H (1989) J Chem Phys 90:1730–1734
14. Cundari TR, Stevens WJ (1993) J Chem Phys 98:5555–5565
15. Ross RB, Gayen S, Ermler WC (1994) J Chem Phys 100:8145–8155
16. Dolg M, Stoll H (1989) Theor Chim Acta 75:369–387
17. Dolg M, Fulde P, Küchle W, Neumann CS, Stoll H (1991) J Chem Phys 94:3011–3017
18. Cao XY, Dolg M (2001) J Chem Phys 115:7348–7355
19. Cao XY, Dolg M (2002) J Mol Struct (Theochem) 581:139–147
20. Perottoni CA, Pereira AS, da Jornada JAH (2000) J Phys (Condensed Matter) 12:7205–7222
21. Pisani C, Dovesi R (1980) Int J Quantum Chem 17:501–516
22. Dovesi R, Pisani C, Roetti C, Saunders VR (1983) Phys Rev B 28:5781–5792
23. Dovesi R (1986) Int J Quantum Chem 29:1755–1774
24. Pisani C, Dovesi R, Roetti C (1996) Hartree–Fock ab-initio treatment of crystalline systems. Lecture Notes in Chemistry. Springer, Berlin Heidelberg NewYork
25. Kalvoda S, Dolg M, Flad HJ, Fulde P, Stoll H (1998) Phys Rev B 57:2127–2133
26. Saunders VR, Dovesi R, Roetti C, Orlando R, Zicovich-Wilson CM, Harrison NM, Doll K, Civalleri B, Bush IJ, D'Arco Ph, Llunell M (2003) CRYSTAL2003 1.0 User's Manual, August 7
27. Dolg M, Stoll H, Preuss H (1993) Theor Chim Acta 85:441–450
28. Pitzer RM (1979) Atomic electronic structure code ATMSCF. The Ohio State University, Columbus
29. Froese Fischer C (1977) The Hartree–Fock method for atoms program MCHF. Wiley, New York. Modified version for pseudopotential and quasirelativistic calculations by Dolg M (1987)
30. Becke AD (1993) J Chem Phys 98:5648–5652
31. Perdew JP, Yue W (1986) Phys Rev B 33:8800–8802
32. Perdew JP (1989) Phys Rev B 40:3399–3399
33. Perdew JP, Wang Y (1992) Phys Rev B 45:13244–13249
34. Perdew JP (1991) Electronic structure of solids. Akademie Verlag, Berlin
35. Han YK, Hirao K (2000) Chem Phys Lett 318:453–458
36. Petukhov AG, Lambrecht WRL, Segall B (1996) Phys Rev B 53:4324–4339
37. Monkhorst HJ, Pack JD (1976) Phys Rev B 13:5188–5192
38. Zicovich-Wilson CM Departamento de Fisica, Universidad Autonoma del Estado de Morelos, http://www.crystal.unito.it/LoptCG/LoptCG.html
39. Causà M, Dovesi R, Pisani C, Roetti C (1986) Phys Rev B 33:1308–1316
40. MOLPRO is a package of ab initio programs written by Werner HJ and Knowles PJ, with contributions from Amos RD, Berning A, Cooper DL, Deegan MJO, Dobbyn AJ, Eckert F, Hampel C, Hetzer G, Leininger T, Lindh R, Lloyd AW, Meyer W, Mura ME, Nicklass A, Palmieri P, Peterson K, Pitzer R, Pulay P, Rauhut G, Schütz M, Stoll H, Stone AJ, Tarroni R, Thorsteinsson T and Werner HJ
41. Wilson LC, Levy M (1990) Phys Rev B 41:12930–12932
42. Perdew JP (1986) Phys Rev B 33:8822–8824
43. MüllerBu H, Vonschne HG (1965) Z Anorg Allg Chem 340:232
44. MüllerBu (1966) Z Anorg Allg Chem 343:6
45. Erying L, Holmberg B (1963) Advanced in chemistry series, American Chemical Society, Washington, vol 39, p 46
46. Frenking G, Antes I, Böhme M, Dapprich S, Ehlers AW, Jonas V, Neuhaus A, Otto M, Stegmann R, Veldkamp A, Vyboishchikov SF (1996) Rev Comput Chem 8:63
47. Koch W, Holthausen MC (2001) A chemist's guide to density functional theory, 2nd edn. Wiley-VCH Verlag, Weinheim
48. Hirosaki N, Ogata S, Kocer C (2003) J Alloys Comp 351:31–34
49. Wang YX, Dolg M (1998) Theor Chem Acc 100:124–133
50. Martin WC, Zalubas R, Hagan L (1978) Atomic energy levels – the rare earth elements, NSRDS-NBS-60, National Bureau of Standards, US Department of Commerce
51. D'Arco P, Sandrone G, Dovesi R, Orlando R, Saunders VR (1993) Phys Chem Minerals 20:407–414
52. Causà M, Dovesi R, Roetti C (1991) Phys Rev B 43:11937–11943
53. Aprà E, Causà M, Prencipe M, Dovesi R, Saunders VR (1993) J Phys (Condensed Matter) 5:2969–2976
54. Gmelin Handbuch der Anorganischen Chemie (1974) Seltenerdelemente; Springer-Verlag, Berlin, Teil C1, 119
55. Schiller G (1985) Dissertation Universität Karlsruhe, pp 1–110
56. Bärnighausen H, Schiller G (1985) J Less-Common Metals 110:385–390
57. Greis O, Ziel R, Breidenstein B, Haase A, Petzel T (1992) J Alloys Compd 216:255–258
58. Faucher M, Pannetier J, Charreire Y, Caro P (1982) Acta Crystallogr B 38:344–346
59. Lide DR (2000–2001) Handbook of physics and chemistry, 81st edn., pp 9–63
60. Chandrasekharaiah MS, Gingerich KA (1989) Handbook on the physics and chemistry of rare earths, North-Holland, Amsterdam, vol. 12, p 409